Hindawi
Advances in Civil Engineering
Volume 2023, Article ID 9033754, 13 pages
https://doi.org/10.1155/2023/9033754

Research Article

Flexural Response of Prestressed FRP Strengthened Reinforced Concrete Beam under Static Load

Utino Worabo Woju[1] **and Biruk Ambachew Asres**[2]

[1]*Department of Civil Engineering, Wachemo University, P.O. Box 667, Hosanna, Ethiopia*
[2]*Department of Civil Engineering, Dire Dawa University, P.O. Box 1362, Dire Dawa, Ethiopia*

Correspondence should be addressed to Utino Worabo Woju; utinoworabo@gmail.com

Received 21 May 2023; Revised 20 July 2023; Accepted 27 July 2023; Published 16 August 2023

Academic Editor: Paolo S. Valvo

Copyright © 2023 Utino Worabo Woju and Biruk Ambachew Asres. This is an open access article distributed under the Creative Commons Attribution License, which permits unrestricted use, distribution, and reproduction in any medium, provided the original work is properly cited.

The motive of building sustainable structures and strengthening the structural members is important to overcome the problems associated with poor initial design and/or construction, accidental events, and degradation related to the environment. This paper aims to assess the flexural behavior of a prestressed basaltic fiber-reinforced polymer- (FRP-) strengthened reinforced concrete (RC) beam under static load through the finite-element method using ABAQUS CAE that is validated with experimental results from relevant literature. To achieve the desired objective, 18 models were prepared based on prestressing level, thickness of basalt FRP (BFRP), width of BFRP, length of BFRP, bond between concrete and BFRP, and type of FRP as study parameters. The results indicate that the use of prestressed BFRP is efficient in strengthening the flexural strength of the RC beam. Compared to nonstrengthened specimens, the flexural capacity of the specimens strengthened with BFRP at prestressing levels of 0%, 15%, 35%, and 45% show enhancement of 6.09%, 9.17%, 13.89%, and 17.57%, respectively. While increasing the width, length, and thickness of the prestressed BFRP section, increased yielding and ultimate load capacity of the specimen have been obtained; however, the ductility has been reduced up to 13.87% with increasing the BFRP thickness. The result also shows that the specimen strengthened with prestressed BFRP has better ductility than the prestressed carbon FRP (CFRP)-strengthened specimen; however, the model strengthened with prestressed CFRP has shown higher load-carrying capacity. It is also noticed that a cohesive bond better suited the experimental specimen than the fixed interference of the concrete surface, and relative to the cohesive bond, the fixed interference has shown a 17.4% higher ultimate load carrying capacity.

1. Introduction

The motive of building sustainable structures and strengthening the structural members has been one of great importance for over a decade to overcome the problems associated with poor initial design and/or construction, accidental events like fire, and degradation related to the environment on structural members like beams, slabs, and columns. While building a sustainable world forces environmentally resistant materials, the utilization of advanced composite fabrics like fiber-reinforced polymers (FRPs) for strengthening structural members has been found suitable [1]. With methods of strengthening and material types always in a state of evolution, techniques of using externally bonded prestressed FRP laminas have become a main fixate for better utilization of the high tensile strength of composite material. Simple externally bonded reinforcement (EBR) has been the main strengthening approach, that is, FRP plates are bonded on the external surface tension side of elements with a bonding agent. But due to early deboning failure, the full tensile strength of FRP can hardly be utilized. To improve the utilization efficiency of the FRP materials, the prestressed FRP strengthening method was introduced as an alternative that offers advantages. Such as reducing deflection and cracking, delaying cracking initiation, and increasing the utilization efficiency of the FRP material [2, 3].

Being widely utilized in the prestressed FRP strengthening approach, carbon FRP (CFRP) with high creep rupture stress is the most widely used FRP material. However, for large-scale applications, its usage is restricted because of its

high cost and brittle behavior, and basaltic fiber (BFRP) has become the new competitive substitute for the benefits it has. Aramid FRP (AFRP) and glass FRP (GFRP) are unsatisfactory as prestressing materials: the former has a large relaxation rate in addition to being expensive, and with less than 30% of the tensile strength, the latter has a low creep rupture stress. Basalt FRP (BFRP) is a new type of environment-friendly and economical material. It has become a competitive substitute for CFRP. It is a green and high-tech fiber product without environmental pollution [3]. Moreover, BFRP exhibits good mechanical properties, acid-alkali resistance, and excellent electrical properties. In addition, compared to carbon fiber, aramid fiber, and glass fiber, basalt shows high wave permeability and excellent sound insulation [4].

Compared with the conventional CFRP laminate, BFRP exhibits a larger failure strain but a lower modulus, in addition to its high strength and prominent creep rupture behavior. This makes BFRP a suitable option for cost-effectively strengthening existing beams. Specimens strengthened with BFRP laminate could achieve 85% of the loading capacity of specimens strengthened with CFRP laminate under the same laminate section and but ensured a superior crack control effect and ductility. Meanwhile, a higher prestressing level leads to a higher material utilization of BFRP [1]. Experimental studies for BFRP and numerical studies for carbon fiber show the bond between FRP and concrete surface, prestressing level, and thickness of FRP have a great influence on the flexural response of the beam [3, 5]. Increasing the level of prestress in the CFRP from 50% to 75% reduced the strength of the beam because the highly prestressed laminates had little strain capacity remaining and the CFRP presented premature failure [6].

To determine the response of prestressed FRP-strengthened reinforced concrete (RC) members, experimental testing is the most widely used method. Yet due to the time-consuming process and the expense method, numerical approaches are handy. The nonlinear behavior of complex and composite materials as well as the prestressing technique can be modeled using nonlinear finite-element methods (FEMs) for a detailed study while minimizing cost and time compared to experimental studies. However, being a relatively newcomer, *further* studies are required to characterize the behavior of BFRP material as an externally bonded strengthening material. This research aims to undergo an assessment of the flexural behavior of RC beams strengthened with prestressed BFRP laminate under gradually incremental static loads and look at the effect of different parameters on the flexural performance of the strengthened beams. Besides, the implementation of such enhanced structure and material properties is especially important for Ethiopia, where most structures and old heritages need retrofitting and buildings with poor initial design and/or construction and those built using old code need strength assessment and improvement. The assessment of BFRP as a strengthening material is effective as it is the most abundant, available raw material for possible production and use.

The section of the specimen is modeled using the advantage of symmetry by modeling only half of the specimen to minimize computation time. And, for simplification, a bilinear approximation is used to model the rebar.

2. Nonlinear Finite-Element Analysis (NLFEA)

A numerical technique to find an approximate solution to boundary value problems involves developing mechanical models that, in turn, reduce the time as well as the cost of experimental tests. Using NLFEA, the performance of the structure under ultimate limit-state conditions can be verified. For this study, the model was developed using the computer program ABAQUS CAE.

2.1. Validation of the NLFEA

2.1.1. Model Geometry and Boundary Conditions. To validate the proposed method, the experimental setup of the model's boundary condition and geometry in this study is obtained from reference [3]. As shown in Figure 1(a), simply supported T-section RC beam specimens loaded in 4-point bending had a total span of 5.2 m, a net span of 5,000 mm, and a pure bending span of 1,100 mm. The cross-section of the beams was a T-type with a height of 350 mm, a flange width of 500 mm, a flange thickness of 100 mm, and a web width of 350 mm, and the BFRP laminate had a section of 50 mm × 2 mm.

The section of the specimen is modeled using the advantage of symmetry by modeling only half of the specimen to minimize computation time. A displacement control general static is used to simulate the 4-point bending test to avoid stress concentration and ensure the uniform distribution of applied displacement. A steel plate of 50 mm thickness modeled as a solid 3D element type is placed on top and at the bottom of the specimen for loading and supporting points, respectively.

2.1.2. Material Modeling. In this study, the behavior of the nonlinear material, the steel, and the concrete uniaxial behaviors after the elastic range are required to be defined. ABAQUS provides different types of concrete constitutive models including: (1) a smeared crack model; (2) a discrete crack model; (3) a damage plasticity model [7]. This study used a concrete damage plasticity (CDP) model for the concrete, and the BFRP plate was modeled as linear elastic, while
the bilinear hardening model is for steel reinforcement. Experimental tests show the behavior of concrete under uniaxial compression to be highly nonlinear and complex. A complete modeling of concrete is expected to capture both its compressive and tension behavior. When it comes to finite-element modeling using ABAQUS, the nonlinear analysis of concrete is mostly carried out using the concrete damaged plasticity approach [7]. This study used a CDP model for the concrete.

Damage properties are sub-optional in ABAQUS and refer to the deterioration of the unloading/reloading stiffness of the martial under cyclic loading. This damage factor d is defined as the reduction of secant modulus relative to the initial elastic modulus at a given point and is a function of the stress state and the uniaxial compressive and tensile damage

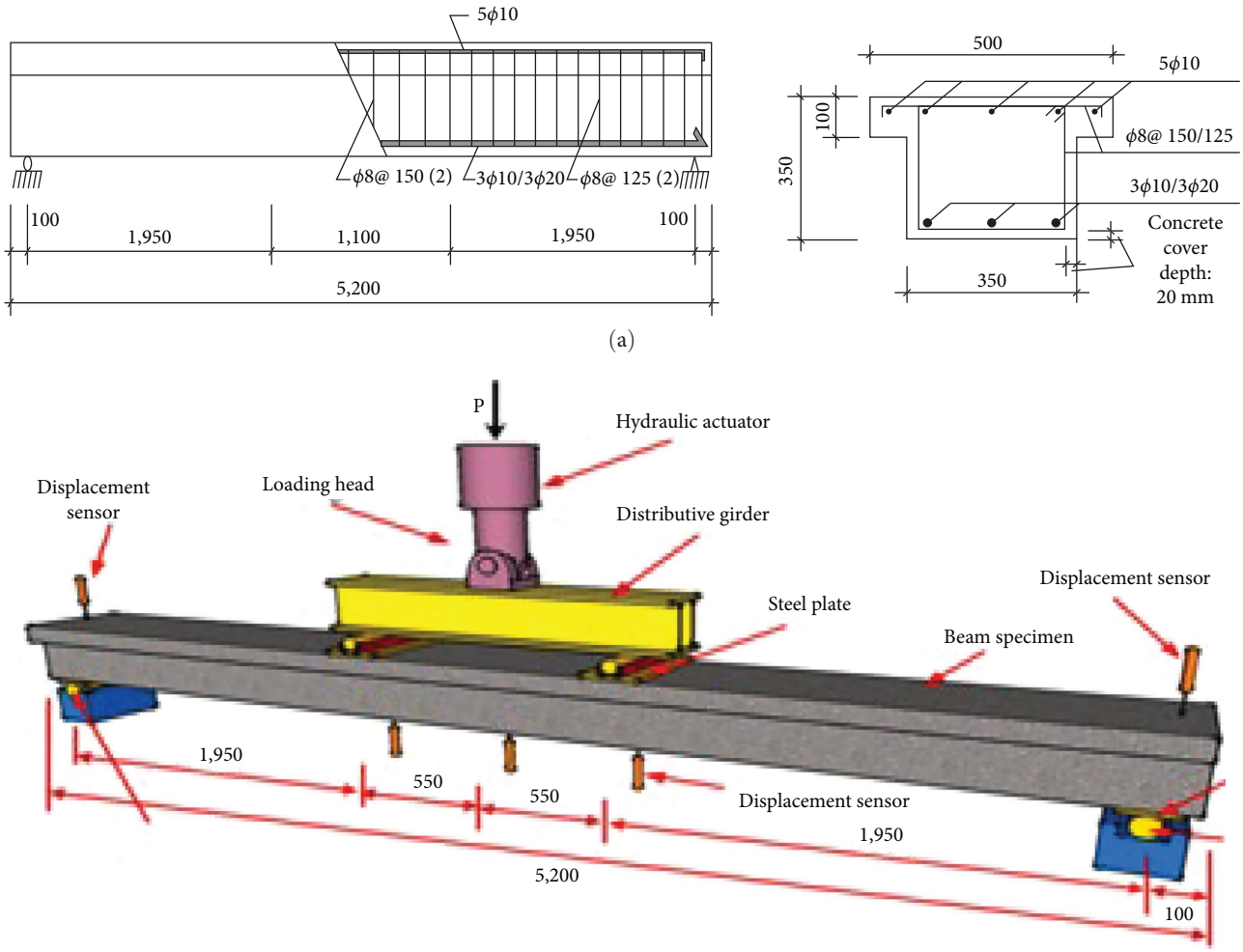

FIGURE 1: Geometry, boundary and cross-section detail of control specimen [3]. (a) Detail and (b) laboratory setup.

variables d_t and d_c [8]. This property is a sub-option in the CDP model, and it can be ignored when dealing with monotonic loading. The compressive elastic, inelastic strain, damage, and equivalent compressive plastic strain are calculated by using Equations (1)–(4).

$$\varepsilon_{0c}^{\mathrm{el}} = \frac{\delta_c}{E_0}, \tag{1}$$

$$\varepsilon_c^{\mathrm{in}} = \varepsilon - \varepsilon_{0c}^{\mathrm{el}}, \tag{2}$$

$$d_c = 1 - \frac{\delta_c}{\delta_{\mathrm{cu}}}, \tag{3}$$

$$\varepsilon_c^{\mathrm{pl}} = \varepsilon_c^{\mathrm{in}} - \frac{d_c}{(1-d_c)}\frac{\delta_c}{E_0}, \tag{4}$$

where $\varepsilon_c^{\mathrm{in}}$ is the compressive inelastic strain; $\varepsilon_{0c}^{\mathrm{el}}$ is the elastic compressive strain corresponding to the initial elastic modulus; $\varepsilon_c^{\mathrm{pl}}$ is equivalent to compressive plastic strain; and d_c is the compressive damage factor.

The strain input to the model is inelastic strain; moreover, the corresponding equivalent plastic strain that controls the evolution of the yield surface needs to be greater than zero, and as the damage factor increases, it should be increasing [8]. In the CDP model, the constitutive relationship of concrete is not given, as it is up to the ABAQUS user to define the constitutive relationship. A numerical expression developed by Hognestad that treats the ascending part as a parabola and the descending part as a straight line [9] is used to drive the material property of concrete. The concrete property in compression is derived by using Equation (5).

$$\begin{aligned} \frac{\sigma}{\sigma_{\mathrm{cu}}} &= 2\frac{\varepsilon}{\varepsilon_0}\left(1 - \frac{\varepsilon}{2\varepsilon_0}\right) \text{ for } 0 < \varepsilon < \varepsilon_0 \\ \frac{\sigma}{\sigma_{\mathrm{cu}}} &= 1 - 0.15\left(\frac{\varepsilon - \varepsilon_0}{\varepsilon_{\mathrm{cu}} - \varepsilon_0}\right) \text{ for } \varepsilon_0 < \varepsilon < \varepsilon_{\mathrm{cu}} \end{aligned}, \tag{5}$$

$$\varepsilon_0 = \frac{2f'_c}{E_c}, \tag{5a}$$

$$\sigma_{c0} = 0.3f'_c, \tag{5b}$$

$$E_0 = 4730\sqrt{f'_c}, \tag{5c}$$

where ε_0 is the strain corresponding to maximum compressive stress; E_0 is the modulus of elasticity of concrete; σ_{c0} is the compressive stress at the onset of plastic deformation σ_{cu} is the maximum compressive strength of concrete; and ε_{cu} is the ultimate compressive strain, 0.0035.

The stress-cracking displacement relation is dependent on the energy required to open a unit area of the crack. The fracture energy G_f, that is, the energy required to create a unit area of the stress-free crack surface that is size independent, instead of the descending branch of the stress–strain curve, which is size dependent, in other words, fracture energy is a material property that is not dependent on the mesh element size. For the particular model, the material property of concrete in tension is modeled by using fracture energy, and using the stress–displacement approach as shown in Equation (6), the concrete property in tension is derived by using [10].

$$\frac{\sigma}{f_t} = f(w) - \frac{w_t}{w_{cr}}(1 + c_1^3)e^{-c_2}, \tag{6}$$

$$f(w) = \left[1 + \left(\frac{c_{1w}}{w_{cr}}\right)^3\right]\exp\left(-\frac{c_{2w}}{w_{cr}}\right), \tag{6a}$$

$$w_{cr} = 5.14\frac{G_f}{f_t}, \tag{6b}$$

$$G_f = 73 \times f_{cm}^{0.18}, \tag{6c}$$

$$f_t = 0.33\sqrt{f_c'}, \tag{6d}$$

where w_t is the crack opening displacement; w_{cr} is the crack opening displacement at the complete loss of tensile stress; σ_t is the tensile stress normal to the crack direction; f_t is the concrete uniaxial tensile strength; and $c_1 = 3.0$ and $c_2 = 6.93$ are constants determined from tensile tests of concrete.

The dilation angle ψ and eccentricity λ are parameters connected with the yield surface flow rule. K_c is the parameter that controls the shape/state of the yield surface. f_{b0} is the concrete biaxial compressive strength; f_{c0} is the uniaxial compressive strength; and the ratio of the two is taken as the suggested esteem. μ is the viscous parameter defined by the CDP model where the bigger μ is, the simpler it is to join/converge. The smaller μ is the higher the exactness is [8].

Steel can be modeled as a bilinear approximation using yielding stress at plastic strain zero and its ultimate strength at any location of strain, or it is possible to use approximately linear elastic material behavior by defining its yielding stress. The mechanical properties of the reinforcing bars with 8, 10, and 20 mm having an elastic modulus of 178, 204, and 197 GPa and yield strengths of 334, 495, and 433 MPa, respectively, and Poisson's ratio, $\nu = 0.3$, have been used.

Being a composite material, FRPs behave essentially as orthotropic. For a unidirectional FRP in a case where the composite is primarily stressed in the fiber direction, the modulus in the fiber direction is probably the more important parameter; hence, an isotropic model is considered suitable [11, 12]. In this study, the FRP plate was modeled as linear elastic, where the stress–strain curve of FRP is assumed to be linear up to when the failure stress is reached. For unidirectional fiber-reinforced composite, a Hashin damage criterion in Abaqus is used to predict the failure of a composite material [13]. For tensile fiber and tensile matrix modes, the failure mode and its analytical description are given respectively as Equations (7) and (8).

$$\left(\frac{\sigma_{11}}{\sigma_{+A}}\right)^2 + \left(\frac{\sigma_{12}}{T_A}\right)^2 = 1 \text{ for } \sigma_{11} > 1, \tag{7}$$

$$\left(\frac{\sigma_{22}}{\sigma_{+T}}\right)^2 + \left(\frac{\sigma_{12}}{T_A}\right)^2 = 1 \text{ for } \sigma_{22} > 0, \tag{8}$$

where σ_{11} is the stress components in fiber direction; σ_{22} is transverse to fibers; σ_{12} is the in-plane or axial shear; σ_{+A} is the tensile failure stress in fiber direction; T_A is the axial failure shear stress; and σ_{+T} is the tensile failure stress transverse to the fiber direction.

The thickness of FRP is 2 mm, and the mechanical properties, elastic modulus and tensile strength of BFRP are 53 GPa and 1,339 MPa, respectively, whereas the elastic modulus and tensile strength of CFRP are 168 and 3,212 GPa, respectively.

2.1.3. Interaction between Materials. An embedded constraint in the interaction module is usually used to create interaction between reinforcing bar and concrete [7]. For this model, the embedment constraint is used where the steel reinforcement was modeled as embedded Regions in the concrete that is the host element; thus, reinforcing elements are only able to make translations or rotations equal to those of the host elements surrounding them.

2.1.4. FRP-Concrete Interfacial Behavior. In the case of numerical modeling using ABAQUS, to represent the interface between concrete and FRP, two different models are used. In the first one, the interface is modeled as a perfect bond, while in the second, it is modeled using a cohesive zone model [14]. A simple bilinear traction separation law is used to model the deboning failure between the concrete surface and the FRP in terms of the effective traction τ and effective opening displacement. The interface is modeled as a rich zone of thin thickness and the initial stiffness K_o is defined as Equation (9).

$$K_o = \frac{1}{\frac{t_i}{G_i} + \frac{t_c}{G_c}}, \tag{9}$$

where t_i is the resin thickness; t_c is the concrete thickness; G_i and G_c are the shear modulus of resin and concrete, respectively; t_c is the concrete thickness, mm, taken $t_c = 5$ mm; G_c is the shear modulus of concrete that is given by $G_c = E/[2(1+\nu)]$, G_{expoy} is the shear modulus of epoxy or adhesive, which is taken as $G_{epoxy} = 665$ MPa. When the opening displacement, $\delta = \delta_0$, the stiffness $K_0 = K_{ss} = K_{tt}$, in which K_{nn} (in the normal direction), K_{ss} and K_{tt} (in the tangential

direction), these stiffness estimated from experimental coupon testing of the epoxy-concrete interface as peeling test for normal stiffness, K_{nn} and Lap joint test for shear stiffness, K_{ss} is equal to K_{tt}.

$$K_{nn} = \frac{1}{\frac{t_c}{E_c} + \frac{t_{expoy}}{E_{expoy}}}, \tag{10}$$

where t_c is the concrete thickness in mm, taken as 5 mm; t_{expoy} is the epoxy or adhesive thickness in mm, taken as 1 mm; E_c is Young's modulus of concrete in MPa; and E_{expoy} is Young's modulus of adhesive in MPa. The approximate value of $K_{nn} = 170$.

The relationship between the traction stress and effective opening displacement is defined by the stiffness, K_o, the local strength of the material, K_{nn}, a characteristic opening displacement at fracture, δ_f, and the energy needed for opening the crack, G_{cr}, which is equal to the area under the traction–displacement curve.

$$\tau_{max} = 1.5\beta f_{ct}, \tag{11}$$

in which $\beta = \sqrt{\left(1.25 - \frac{b_f}{b_c}\right) / \left(1.25 + \frac{b_f}{b_c}\right)}$; b_f is the FRP plate width, b_c is the concrete width and f_{ct} is the concrete tensile strength.

Reducing the value of τ_{max} accelerates the de-bonding of FRP sheets. The damage evolution law describes the rate at which the material stiffness is degraded once the corresponding initiation criterion is reached. Different models are available in ABAQUS, such as evolution based on energy or evolution based on effective displacement. Normal Fracture Energy = 0.09 mJ/mm^2, 1st Shear Fracture Energy = 2nd Shear Fracture Energy range from 0.3 to 1.5 mJ/mm^2. Usually take = 0.9 mJ/mm^2 or computed from the area under traction–separation curve (Gcr) [11, 15]. In this study, both perfect bond and cohesive models were utilized to model the interface between BFRP concrete surfaces.

2.1.5. Modeling of Prestressing Effect. Two approaches are known to be used to simulate the prestressing effect in ABAQUS, which is by using initial stress or initial temperature load. The former defines the intensity of the stresses, where the letter uses an equivalent temperature load to stress, and the applied temperature t (°C) can be obtained from Equation (12).

$$C = -\frac{P}{C.E.A} \tag{12}$$

where C is the coefficient of linear expansion in (MPa/°C); E is the modulus elasticity of the material, in MPa; A is the cross-sectional area of the prestressing section in mm^2; P (in N) is prestressing force calculated based on the recorded force during pretension process and with consideration of loss of prestressing effect [7, 16]. For this study, the initial temperature load is used to apply the prestressing load with a thermal expansion of BFRP of 8×10^{-6}/°C and -9×10^{-6}/°C for CFRP.

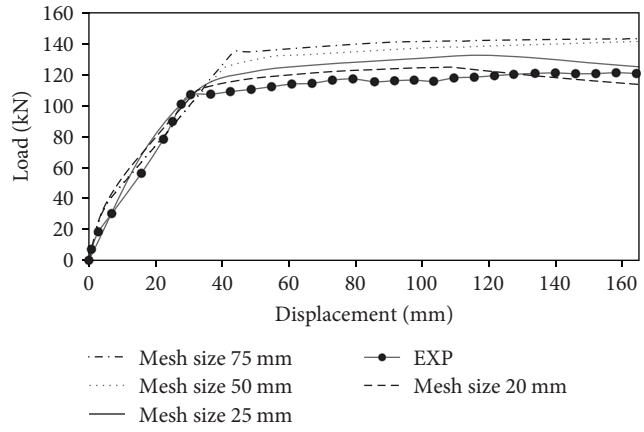

Figure 2: Shows mesh sensitivity.

2.1.6. Mesh Sensitivity Analysis. It is not convent and computationally efficient to obtain a solution for a region by considering infinite small-size elements; hence, to make it finite, a region is discretized into finite elements and simulation is carried out as such. The core idea of meshing is to find a solution at limited points (nodes) and interpolate the result for the other points in the element through the interpolation function (shape function).

The accuracy of results in FEA analysis is influenced by the degree of discretization of elements and mesh size. Different sizes, that is, 20, 25, 50, and 75 mm, were tried on before concluding the final element mesh size as shown in Figure 2. However, the yielding load and ductility index of mesh sizes 20 and 25 mm are equal to the experimental result, and the pre-peak response of mesh sizes 25 mm has a good fit with the experimental result. Besides, the computational efficiency of a 25 mm mesh size is better than that of a 20 mm mesh size. Thus, a mesh size of 25 mm × 25 mm × 25 mm in all dimensions is used, as it is found to be fine enough to obtain the desired result, as shown in Figure 2. The model contained 22256 C3D8R elements for concrete, 272 linear line elements of type T3D2 for steel reinforcement, and 200 linear quadrilateral elements of type S4R for FRP.

2.1.7. Validation of Finite-Element Analysis (FEA). The load-deflection diagrams of both the experimental test and FEA for the controlled beam (D-20-CON) and prestressed BFRP strengthened beam (D20-B2-P45-Y) are presented, respectively. In Figure 3, it is observed that the FEA model was able to reasonably match the experimental result of [3] with respect to yield and ultimate load. Compared with the experimental result, the discrepancy between yield load, Py, and ultimate load capacity, Pu, of D20-CON is 6.1% and 8.8%, respectively, whereas that of D20-B2-P45-Y is 5.8% and 3.2%, respectively.

It is possible to consider that the cracks develop where the maximum principal strain is positive since CDP is limited in grasping the crack pattern at material integration points. To contrast the crack marking of the model, visualizing the plastic strain distributions obtained from the FEA with the crack patterns obtained from the experiments is

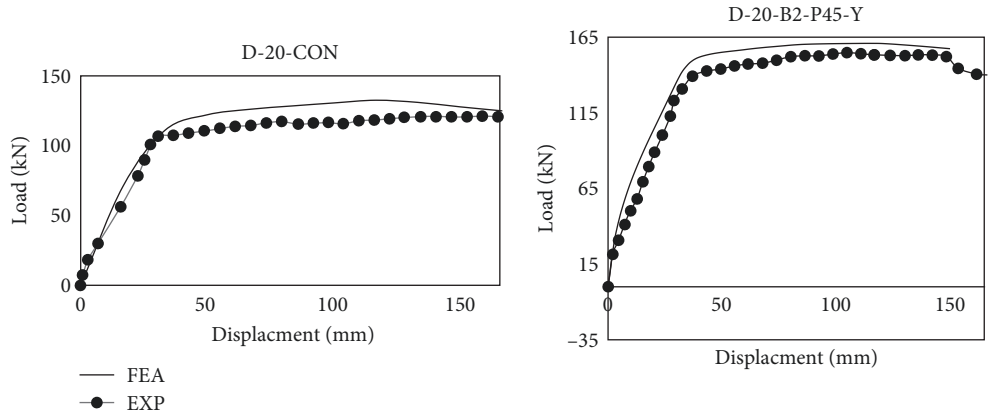

Figure 3: Load versus displacement of experimental and finite-element analysis (FEA) results.

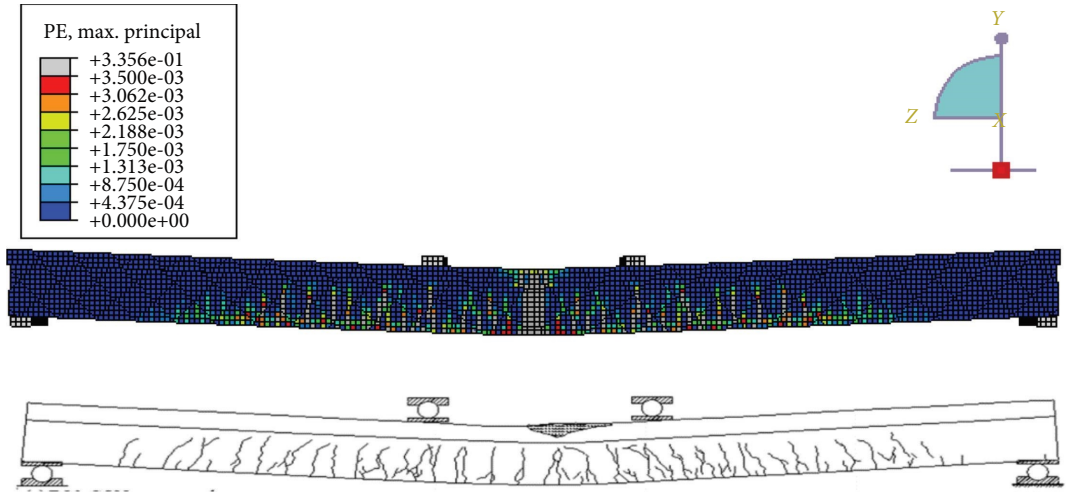

Figure 4: Comparison between crack patterns of finite element model and experimental analysis.

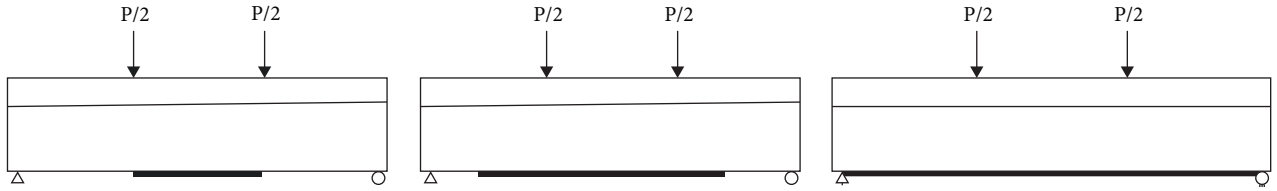

Figure 5: Typical FEA model showing length of basalt fiber-reinforced polymer (BFRP) laminate 1.1, 3.9, and 5 m, respectively.

mostly used [12, 17, 18]. Hence, using the mirror view in ABAQUS to better visualize the full model, Figure 4 shows that the control beam general crack pattern of the FEA model appreciably fits with the experimental 1. That shows the mechanisms of fracture in the beam are well represented in the model.

3. Parametric Study

To characterize prestressed basaltic fiber-strengthened RC beam and assess how BFRP material behaves as externally bonded strengthening material, numerical simulations were conducted on the provided model. To investigate the effects of different parameters on a prestressed BFRP-strengthened RC beam. The studied parameters of the model were: (i) prestressing level, (ii) thickness of FRP, (iii) width of FRP, (iv) length of FRP(mm) as shown in Figure 5, (v) type of FRP, and (vi) bond between FRP and concrete. Details of each specimen are provided in Table 1. And, other than the control specimen (SP-CON), each FEM is assigned a unique designation letter as SP-(N)-X-T/L/W–K, where SP is to denote specimen; (N) denotes the EBR laminate or the pre-stressed laminate with a prestressing level of 15% fu, 35% fu, or 45% fu (P15, P35, or P45); and fu is the tensile strength of the FRP laminate-anchorage assembly as the experimental test which is 1,150 MPa for BFRP laminates and 2,400 MPa

Table 1: Study matrix of finite-element test models.

NO	FEA model designation	FRP type	Prestressing level (%)	Thickness of FRP (mm)	Width of FRP (mm)	Length of FRP (mm)	Bond	Remark
1	SP-CON	–	–	–	–	–	–	Controlled beam
2	SP-EBR-B-2/50/5000–C	BFRP	0	2	50	5,000	Cohesive	Investigating the influence of prestressing level
3	SP-P15-B-2/50/5000–C	BFRP	15	2	50	5,000	Cohesive	
4	SP-P35-B-2/50/5000–C	BFRP	35	2	50	5,000	Cohesive	
5	SP-P45-B-2/50/5000–C	BFRP	45	2	50	5,000	Cohesive	
6	SP-P35-B-2/50/5000–C	BFRP	35	2	50	5,000	Cohesive	Investigating the influence of BFRP thickness
7	SP-P35-B-3/50/5000–C	BFRP	35	3	50	5,000	Cohesive	
8	SP-P35-B-4/50/5000–C	BFRP	35	4	50	5,000	Cohesive	
9	SP-P35-B-2/30/5000–C	BFRP	35	2	30	5,000	Cohesive	Investigating the influence of BFRP width
10	SP-P35-B-2/50/5000–C	BFRP	35	2	50	5,000	Cohesive	
11	SP-P35-B-2/100/5000–C	BFRP	35	2	100	5,000	Cohesive	
12	SP-P35-B-2/50/1100–C	BFRP	35	2	50	1,100	Cohesive	Investigating the influence of BFRP length
13	SP-P35-B-2/50/3900–C	BFRP	35	2	50	3,900	Cohesive	
14	SP-P35-B-2/50/5000–C	BFRP	35	2	50	5,000	Cohesive	
15	SP-P35-B-2/50/5000–C	BFRP	35	2	50	5,000	Cohesive	Investigating the influence of FRP Type
16	SP-P35-C-2/50/5000–C	CFRP	35	2	50	5,000	Cohesive	
17	SP-P45-C-2/50/5000–C	BFRP	45	2	50	5,000	Cohesive	Investigating the influence of bond

FEA, Finite-element analysis; BFRP, basalt fiber-reinforced polymer; CFRP, carbon fiber-reinforced polymer.

Table 2: Load results of the specimen with varying prestressing level.

FEA model designation	Cracking load (kN)	Yield load (kN)	Ultimate load (kN)
SP-CON	13.9	111.37	132.6
SP-EBR-B-2/50/5000–C	20.83	119.5	139.1
SP-P15-B-2/50/5000–C	28.54	124.6	146
SP-P35-B-2/50/5000–C	30.22	132.28	154
SP-P45-B-2/50/5000–C	35.24	147.2	160.87

FEA, Finite-element analysis.

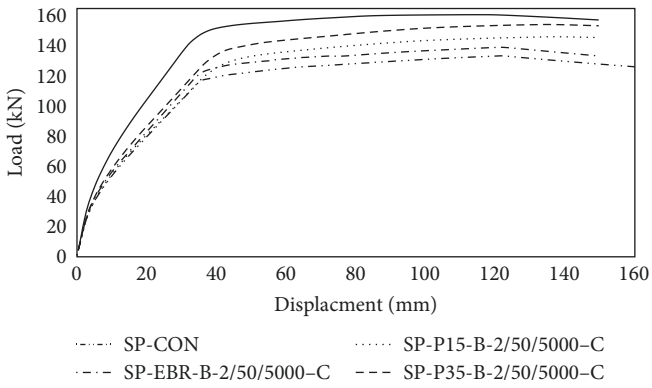

Figure 6: Load versus displacement for different prestressing level.

for CFRP laminates. X is for the type of FRP (C = CFRP or B = BFRP); T, L, and W are the thickness, length and width of BFRP in mm and K indicates the bond between FRP and concrete (C = bonded, F = fixed). For the presented specimens, while all other parameters are held constant the particular investigated parameter is varied.

The result summarizes the study parameters that represent the behavior of specimens concerning the cracking load (P_{cr}), yielding load (P_y), and ultimate load (P_u) and the influence of each parameter.

3.1. Influence of Prestressing Level. The response of the specified specimens was assessed numerically by applying different prestressing levels of 0%, 15%, 35%, and 45%, and the influence of prestressing the BFRP plate on the FEA models was tracked. It is observed that the cracking load, yielding load, and ultimate load-carrying capacity of the model improved with the increasing prestressing level.

As presented in Table 2, compared to the nonstrengthened control specimen, the capacities of the specimens strengthened with BFRP of prestressing levels 0%, 15%, 35%, and 45% have shown enhancements of 6.83%, 10.6%, 15.8%, and 24.3%, respectively, for yielding load and an increment of 4.67%, 9.17%, 13.89%, and 17.57% on the ultimate load carrying capacity, respectively.

The load–displacement curve of the models with the aforementioned specimens is shown in Figure 6, and three parts can be distinguished from the curve. The first part is at the initial loading stage, and it proceeds until the onset of concrete cracking takes place. At this stage of the loading, the curve is linearly elastic and its slope is sharp due to the high stiffness of the specimens at lower displacement, which makes the effect of FRP on the capacity of the beamless, and it can be seen that the stiffness of controlled and strengthened specimens is very close at this stage.

In the second portion of the curve, due to the formation of concrete cracking at the beam's bottom tension zone, as concrete is weak in tension, the concrete will no longer participate in bearing the capacity of the beam, which causes the rate of deflection to get relatively faster. Accordingly, the slope of the curve is slightly decreased, and the stiffness of the specimens is reduced. Moreover, at this stage, the tension stress is resisted by the internal reinforcements and BFRP. As shown in the diagram, the strengthened specimens show better stiffness than the controlled ones, and this part of the load–displacement curve continues until the tensile steel yields. And on the third one, the slope of the curve undergoes a noticeable reduction, and the section becomes soft after the reinforcing steel yields. Therefore. The stress on BFRP increased, and the strengthening played a major role in resisting the load; hence, the strengthened specimens show a higher load resistance, and a higher prestressing has shown a better response.

Increasing the prestressing level has improved the capacity of the specimen. Increasing the prestressing level from 0% to 15% has shown a good improvement in terms of cracking load and a slight improvement in terms of yield and ultimate load-carrying capacity. And further increasing the prestressing level to 35% and 45% has shown a better improvement with respect to the yielding and ultimate load-carrying capacity of the specimen. For a prestressing level of 15%, 35%, and 45%, an improvement of 27.01%, 31.07%, and 40.8%, respectively, with respect to cracking load and a 4.72%, 9.67%, and 13.53% increment, respectively, for the ultimate load obtained in comparison to specimens strengthened with non-prestressed BFRP.

Relative to the non-prestressed BFRP strengthened specimen, the yielding load of internal reinforcements is advanced, with increasing the prestressing level. For the 15% prestressing level an improvement of 4.09% on the yielding load is observed by increasing the prestressing level to 35% and 45% the yielding load of internal reinforcements was improved by 9.6% and 18.8% when compared to the specimen strengthened with non-prestressed BFRP.

Visualizing the plastic strain distributions obtained from the FEA software ABAQUS, It is possible to consider that the cracks develop where the maximum principal strain is positive, it is mostly used to observe the Crack patterns of specimens [12, 17, 18].

For each specimen, the cracks start appearing at the bottom face of the beam at a different level of cracking load and

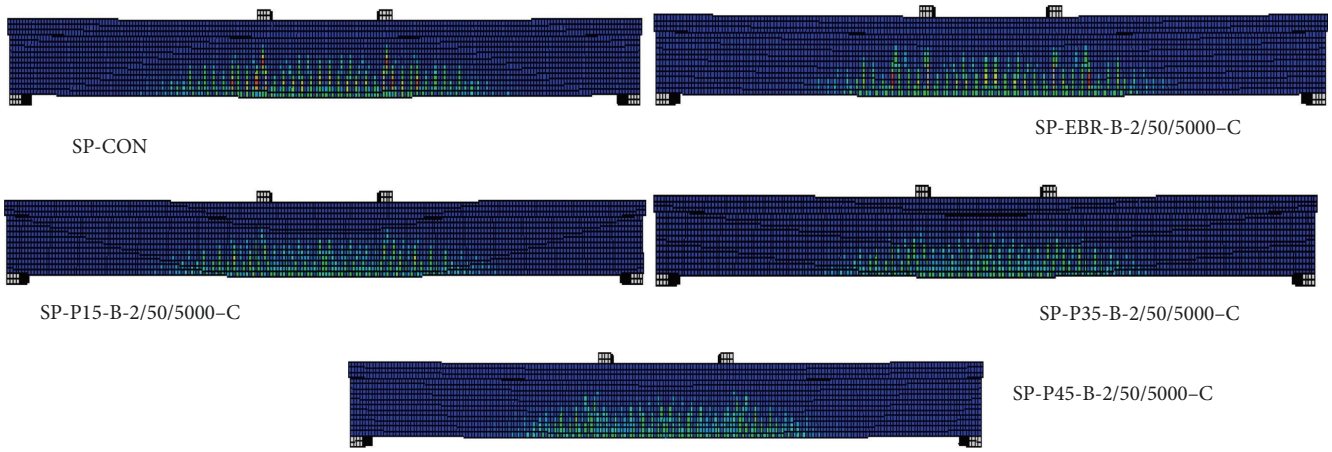

Figure 7: Shows crack pattern of specimens.

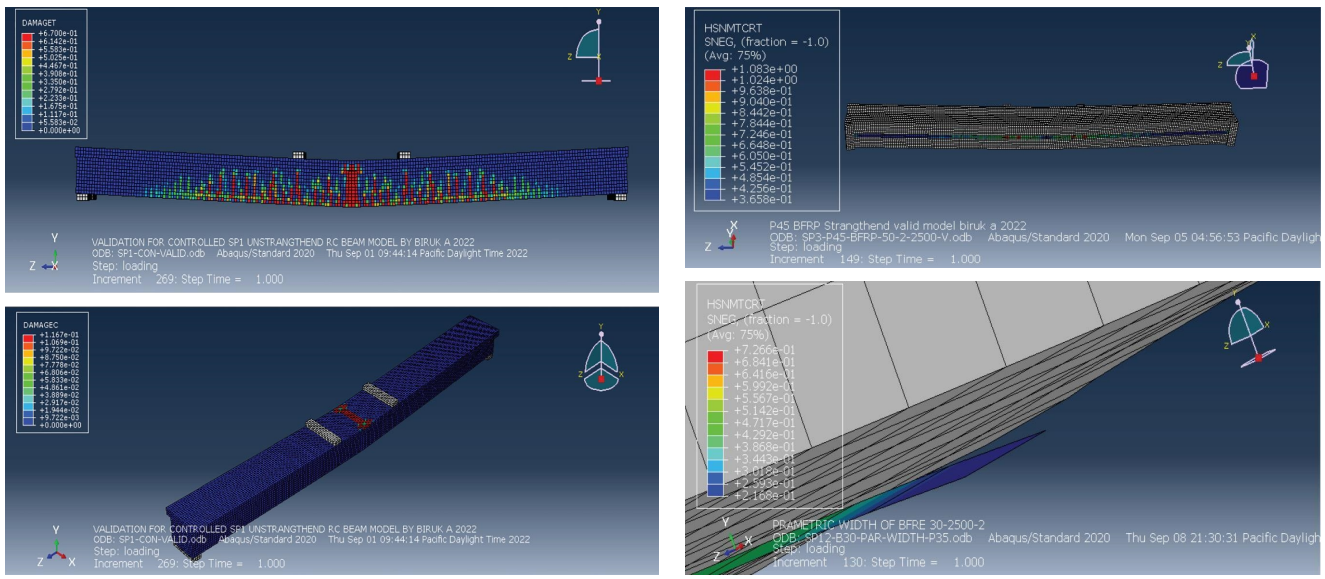

(a) (b)

Figure 8: Shows damage in material (a) concrete damage and (b) BFRP damage.

extended along the tension zone of the beam. The first visible crack was noticed at the midspan flexural region. And additional cracks started to appear as the load level was increasing. For the same load, the specimens strengthened with prestressed BFRP have managed to show a slight restriction on the crack pattern. A denser, less sparse and relatively even crack pattern is shown in Figure 7. For each specimen, the variation in crack patterns could have been more visible on the strengthened RC beams if it was not for the restriction by internal steel reinforcements as stated by Wang et al. [19].

Compared to the control model the specimens strengthened with BFRP of prestressing level 0%, 15%, 35%, and 45% has shown enhancement of the cracking load by 34.7%, 52.3% 54.9%, and 61.4% respectively which shows that the onset of cracking load delayed with increasing the prestressing level.

The control beam in the FEA shows conventional flexural failure mode, that is, where concrete crushing after the yielding of the steel reinforcements. The specimen showing the tensile and compression damages are presented in Figure 8(a) and for the prestressed BFRP strengthened specimens the FEA model has shown a slight partial deboning failure of FRP moreover conventional flexural failure when the loading process continued and partial fracture of BFRP is observed for SP-P45-B-2/50/5000–C model Figure 8(b).

As presented in Table 3 the ductility index shows that the ductility of strengthened beams decreased with an increasing prestressing level on BFRP. Without a significant reduction in load-caring capacity, the ability of the structure to sustain inelastic deformation before failure is called ductility. It indicates the pre-failure nonlinear range of the section when a structural member, material and cross-section of a structure are subjected to loading. the ductility index was considered as the ratio of maximum (failure) mid-span deflection to the first yield deflection of steel, that is, ductility index,

Table 3: Comparison of ductility of the specimens for different strengthened models.

FEA model designation	Δy (mm)	Δu (mm)	Ductility index
SP-EBR-B-2/50/5000–C	33.18	129.4	3.89
SP-P15-B-2/50/5000–C	39.54	132.9	3.36
SP-P35-B-2/50/5000–C	38.88	126.4	3.25
SP-P45-B-2/50/5000–C	36.06	115.57	3.20

FEA, Finite-element analysis.

Table 4: Load results of specimen with varying thickness of prestressed basalt fiber-reinforced polymer.

FEA model designation	Cracking load (kN)	Yield load (kN)	Ultimate load (kN)
SP-CON	13.9	111.37	132.6
SP-P35-B-2/50/5000–C	30.2	132.2	154.3
SP-P35-B-3/50/5000–C	31.52	138.79	159.9
SP-P35-B-4/50/5000–C	35.4	146.07	161.26

FEA, Finite-element analysis.

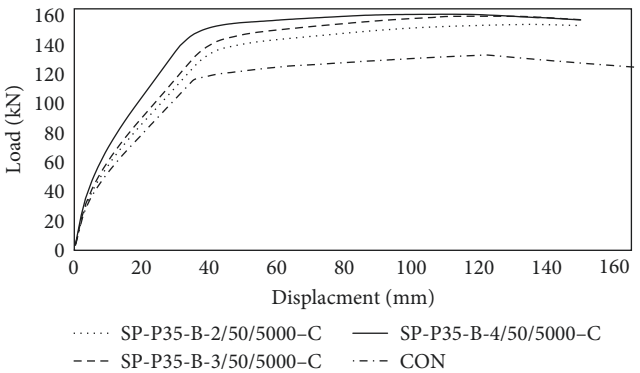

Figure 9: Load versus displacement for different thickness of prestressed BFRP.

$\mu = \Delta_u/\Delta_y$ [20]. In comparison to specimens strengthened with non-prestressed BFRP, models strengthened with prestressed BFRP levels of 15%, 35%, and 45% exhibit a ductility reduction of 13.62%, 16.45%, and 17.7% respectively. The result shows that models strengthened with a higher level of prestressed BFRP exhibit a lower ductility response and reduction of ductility. And this is observed because of the additional tension stiffening increment induced in the beam resulting from prestressing BFRP [3].

3.2. Influence of BFRP Thickness. The influence of the specified specimens under the different thicknesses of prestressed BFRP plate was assessed and it is observed that the cracking load, yielding load and ultimate load carrying capacity of the model was improved with the increasing thickness of prestressed BFRP. The specimen strengthened with thicker laminate has shown better performance in terms of load-carrying capacity. In comparison to the controlled specimen, increasing the thickness of the prestressed BFRP plate as 2, 3, and 4 mm has shown an increment of 14.04%, 17.07%, and 17.7% on ultimate load carrying capacity, respectively, as shown in Table 4 and Figure 9. Increasing the thickness of BFRP improved the capacity of the specimen. Doubling the thickness from 2 to 4 mm thickness of BFRP has shown a 14.6%, 9.49%, and 4.3% and increase for cracking, yield, and ultimate load respectively.

Table 5: Comparison of ductility of the specimens for different thickness of basalt fiber-reinforced polymer.

FEA model designation	Δy (mm)	Δu (mm)	Ductility index
SP-P35-B-2/50/5000–C	38.88	134.9	3.47
SP-P35-B-3/50/5000–C	39.04	118.34	3.02
SP-P35-B-4/50/5000–C	37.39	111.62	2.98

FEA, Finite-element analysis.

As presented in Table 5, the ductility index shows that the ductility of strengthened beams decreased with an increase in BFRP thickness. In comparison to the specimen strengthened with prestressed BFRP of 2 mm thickness, increasing the thickness of the section to 3 and 4 mm has decreased the ductility of the specimen by 12.9% and 13.87%. This reduction of ductility is observed because of the additional tension stiffening of BFRP resulting from thickness increase.

3.3. Influence of BFRP Width. Under different width of prestressed BFRP plates, the response of the model was studied. By increasing the width of the prestressed BFRP plate, the strengthened RC beam has shown an improvement in terms of its yielding and ultimate loads carrying capacity moreover a specimen strengthened with wider BFRP has shown a better stiffness.

Based on the results, relative to the controlled specimen increasing the width of the prestressed BFRP plate as 30, 50, and 100 mm has an increment of 12.59%, 13.9%, and 15.78% for the ultimate load respectively. Figure 10 shows the load–displacement curve of the specimen with the aforementioned BFRP width. Increasing the width of BFRP has slightly improved load resistance capacity of the specimen.

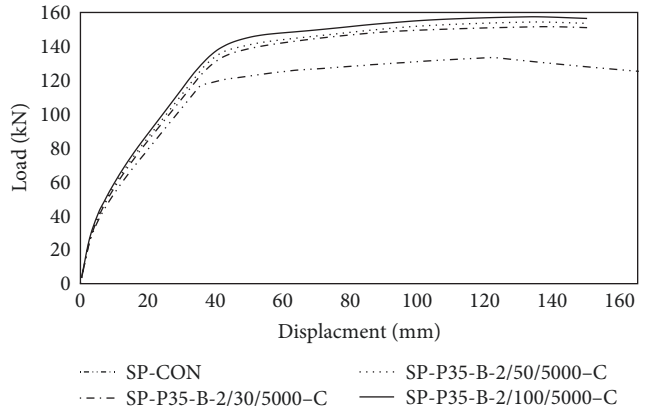

Figure 10: Load versus width of prestressed BFRP.

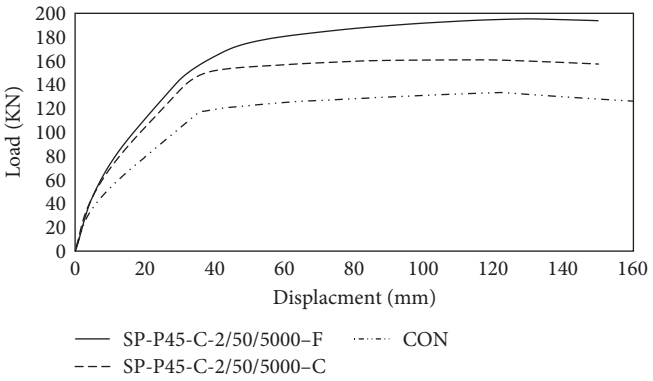

Figure 11: Load versus displacement for the bond influence of prestressed BFRP.

Table 6: Comparison of ductility of the specimens for different width of basalt fiber-reinforced polymer (BFRP) load versus width of prestressed BFRP.

FEA model designation	Δy (mm)	Δu (mm)	Ductility index
SP-P35-B-2/30/5000–C	38.9	137	3.52
SP-P35-B-2/50/5000–C	38.8	134.9	3.47
SP-P35-B-2/100/5000–C	39.97	133	3.32

FEA, Finite-element analysis.

Figure 11 shows that doubling the width from 50 to 100 mm of BFRP has shown a 2.19%, 3.53%, and 3.82% increase for cracking, yield and ultimate load respectively.

As seen in Table 6, the ductility index shows that the ductility of strengthened beams decreased with an increase in BFRP width. In comparison to the specimen strengthened with Prestressed BFRP width of 30 mm, increasing the width of the section to 50 and 100 mm has decreased the ductility of the specimen by 1.4% and 5.6%. And in comparing the effect of thickness to the width of the prestressed BFRP in the ductility reduction.

3.4. Influence of BFRP Length. The response of the specimen has shown that increasing the length of BFRP has influenced the load-carrying capacity. Compared with the controlled

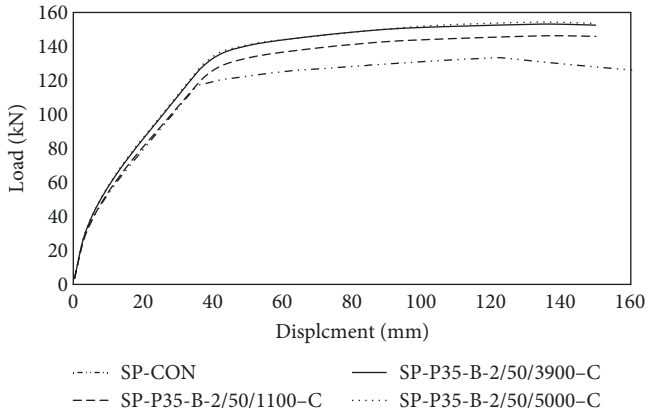

Figure 12: Load versus displacement for different length of prestressed BFRP.

Table 7: Comparison of ductility of the specimens for different length of basalt fiber-reinforced polymer.

FEA model designation	Δy (mm)	Δu (mm)	Ductility index
SP-P35-B-2/50/1100–C	36.7	137.36	3.75
SP-P35-B-2/50/3900–C	37.02	137.02	3.70
SP-P35-B-2/50/5000–C	38.8	134.9	3.47

FEA, Finite-element analysis.

specimen BFRP with a length of 1,100, 3,900, and 5000 mm has shown an increase of 9.3%, 13.3%, and 14.04% for ultimate load capacity respectively. It can also be observed in Figure 12 the specimen strengthened with a higher length of prestressed BFRP has exhibit better stiffness. The result of the specimen shows that by increasing the length of BFRP from 1,100 to 5,000 mm specimen has shown an increase of 37.52%, 9.07%, and 5.18%, increase for cracking, yield and ultimate load respectively.

Moreover, as presented in Table 7, the ductility index of the specimen strengthened for varying prestressed BFRP length and it is observed that the ductility of strengthened beams has shown a reduction with an increase in BFRP length. In comparison to the specimen strengthened with a prestressed BFRP length of 1,100,mm, increasing the length of the section to 3,900 and 5,000 mm has decreased the ductility of the specimen by 1.35% and 7.4%.

3.5. Influence of FRP Type. For the similar section although the CFRP showed a higher load resistance capacity, the specimen strengthened with prestressed BFRP has shown better ductility. As shown in Table 8 specimen strengthened with prestressed CFRP laminate achieved higher load-carrying capacity. In comparison to the specimen strengthened with prestressed BFRP laminate under the same laminate section the specimen strengthened with prestressed CFRP shows a 32.2%, 10.7%, and 2.95% increase in cracking, yielding and ultimate load respectively.

Moreover, as seen in Table 9 the ductility index shows that the specimen strengthened with prestressed BFRP has slightly better ductility than Specimen strengthened with prestressed CFRP. For the model strengthened with prestressed

Table 8: Load results of specimen with varying FRP type of prestressed basalt fiber-reinforced polymer.

FEA model designation	Cracking load (kN)	Yield load (kN)	Ultimate load (kN)
SP-CON	13.9	111.37	132.6
SP-P35-B-2/50/5000–C	30.2	132.23	154.01
SP-P35-C-2/50/5000–C	44.64	148.13	158.7

FEA, Finite-element analysis.

Table 9: Comparison of ductility of the specimens for different fiber-reinforced polymer type.

FEA model designation	Δy (mm)	Δu (mm)	Ductility index
SP-P35-B-2/50/5000–C	38.8	134.9	3.47
SP-P35-C-2/50/5000–C	39.04	132.3	3.38

FEA, Finite-element analysis.

BFRP ductility index has improved by 2.59% in comparison to specimen strength with prestressed CFRP and this increment in ductility can be explained due to the lower modulus of elasticity which gives a relatively larger failure strain for BFRP as stated by Liu et al. [3].

3.6. Influence of Bond. The response of the specimen has shown that the bond between the concrete surface and the BFRP has influenced the model response. The specimens with fixed bond interference have shown a higher estimation of cracking, yielding and ultimate load. Compared with the cohesive model the fixed bond assumption has overestimated the ultimate load-carrying capacity by 17.4% and the specimen strengthened with a fixed bond was unable to represent the debonding mode of failure. It can also be observed in Figure 11 the fixed bond is stiffer than the cohesive bond mode that is due to the perfect bond between the concrete and the BFRP surface.

4. Conclusions

In this study, the influence of the prestressing level, thickness of BFRP, width of BFRP, length of BFRP, bond between concrete and BFRP, and type of FRP on the flexural strength of an RC beam has been investigated using nonlinear FEM. The main findings are concluded as follows:

(1) As compared to the controlled specimen, all the strengthened specimens have shown a higher ultimate load-carrying capacity, and flexural cracks form at lower loads in the control beam. Compared to the controlled specimen, by using a 45% prestressing level of BFRP, the strengthened specimen's ultimate load capacity was enhanced by 17.7%, and the yielding load of internal reinforcements was advanced up to 24.3%.

(2) Increasing the thickness, width, and length of BFRP results in a higher ultimate load-carrying capacity; however, the ductility has been reduced by up to 13.87% with increasing the BFRP thickness.

(3) A wider and thicker section of BFRP sections has a better stiffness response, but a thinner section has a better ductility response. Doubling the width of BFRP from 50 to 100 mm has shown a 2.19%, 3.53%, and 3.82% increase for cracking, yield, and ultimate load, respectively.

(4) Prestressed BFRP has better ductility in comparison to prestressed CFRP, yet a higher load-carrying capacity can be achieved using prestressed CFRP.

(5) The cohesive bond represents the experimental model more accurately than the fixed bond in terms of considering the deboning mode of failure; furthermore, the fixed bond overestimates the ultimate load-carrying capacity of the model.

Data Availability

Data are available upon request.

Conflicts of Interest

The authors declare that they have no conflicts of interest.

Acknowledgments

We would like to thank Wachemo University and Dire Dawa University for uninterrupted monthly salaries and Arba Minch University for the scholarship opportunity.

References

[1] Fib bulletin 14 and FIB TG 9.3 FRPEBR, "Externally bonded FRP reinforcment for RC structures," Federation Internacionale du betun (Fib). Task Group 9.3 FRP, 1-3, 2001.

[2] ACI 440-R07, "Report on fiber-reinforced polymer (FRP) reinforcement (ACI 440-R07)," American Concrete Institute, Farmington Hills, MI, Vol 2007 Reported by ACI Committee 440, 2007.

[3] C. Liu, X. Wang, J. Shi, L. Liu, and Z. Wu, "Experimental study on the flexural behavior of RC beams strengthened with prestressed BFRP laminates," *Engineering Structures*, vol. 233, Article ID 111801, 2021.

[4] C. B. Nayak, G. N. Narule, and H. R. Surwase, "Structural and cracking behavior of RC T-beams strengthened with BFRP sheets by experimental and analytical investigation," *Journal of King Saud University–Engineering Sciences*, vol. 34, no. 6, pp. 398–405, 2022.

[5] M. Daugevičius, "Numerical investigation of RC beams strengthened with prestressed CFRP," *Engineering Structures and Technologies*, vol. 9, no. 3, pp. 148–156, 2017.

[6] M. A. Masuelli, *Fiber Reinforced Polymers—The Technology Applied for Concrete Repair*, InTech, 2013.

[7] W. Ren, L. H. Sneed, Y. Yang, and R. He, "Numerical simulation of prestressed precast concrete bridge deck panels

using damage plasticity model," *International Journal of Concrete Structures and Materials*, vol. 9, pp. 45–54, 2015.

[8] L. Qingfu, G. Wei, and K. Yihang, "Parameter calculation and verification of concrete plastic damage model of ABAQUS," *IOP Conference Series: Materials Science and Engineering*, vol. 794, Article ID 012036, 2020.

[9] S. V. Chaudhari and M. A. Chakrabarti, "Modeling of concrete for nonlinear analysis using finite element code ABAQUS," *International Journal of Computer Applications (0975–8887)*, vol. 44, no. 7, pp. 14–18, 2012.

[10] Y. Tao, J. F. Chen, and M. Asce, "Concrete damage plasticity model for modeling FRP-to-concrete bond behavior," *Journal of Composites for Construction*, vol. 19, no. 1, Article ID 04014026, 2015.

[11] A. Sakbana and M. Mashreib, "Finite element analysis of CFRP-reinforced concrete beams," *Revista Ingeniería de Construcción*, vol. 35, no. 2, pp. 148–169, 2020.

[12] Y. T. Obaidat, "*Structural retrofitting of concrete beams using FRP: debonding issues*," Doctoral thesis, Lund University, 2011.

[13] Z. Hashin, "Failure criteria for unidirectional fiber composites," *Journal of Applied Mechanics*, vol. 47, no. 2, pp. 329–334, 1980.

[14] S. E. Günaslan, A. Karaşin, and M. E. Öncü, "Properties of FRP Materialsfor Strengthening," *IJISET - International Journal of Innovative Science, Engineering & Technology*, vol. 1, no. 9, pp. 656–660, 2014.

[15] Y. T. Obaidat, "*Structural retrofitting of reinforced concrete beams using carbon fibre reinforced polymer*," Licentiate dissertation, Lund University, 2010.

[16] M. Al-Ilani and Y. Temsah, "Comparative study of modeling methods used to simulate initial stresses in prestressed beams towards manual analysis," *MATEC Web of Conferences*, vol. 281, Article ID 01014, 2019.

[17] S. K. Paul and P. Sahu, "Finite element analysis of retrofitting of rc beam with CFRP using abaqus," *International Research Journal of Engineering and Technology (IRJET)*, vol. 7, no. 2, pp. 1268–1273, 2020.

[18] M. A. Al-saawani, A. I. Al-negheimish, A. K. El-sayed, and A. M. Alhozaimy, "Finite element modeling of debonding failures in FRP-strengthened concrete beams using cohesive zone model," *Polymers*, vol. 14, no. 9, Article ID 1889, 2022.

[19] X. Wang, J. Shi, G. Wu, L. Yang, and Z. Wu, "Effectiveness of basalt FRP tendons for strengthening of RC beams through the external prestressing technique," *Engineering Structures*, vol. 101, pp. 34–44, 2015.

[20] N. Jeevan, H. N. Jagannatha Reddy, and R. Prabhakara, "Flexural strengthening of RC beams with externally bonded (EB) techniques using prestressed and non-prestressed CFRP laminate," *Asian Journal of Civil Engineering*, vol. 19, pp. 893–912, 2018.